

# Flow and Fouling in Elastic Membrane

<sup>1</sup>Zhengyi Chen, <sup>1</sup>Shiyue Liu, <sup>2</sup>Rituparna Basak, <sup>3</sup>Mingkai Yu, <sup>3</sup>Ellie Gurvich,  
<sup>4</sup>Naren Vohra, <sup>5</sup>Daniel Jonas, <sup>1</sup>Pejman Sanaei

1 New York University, New York, USA

2 New Jersey Institute of Technology, New Jersey, USA

3 University of Maryland, Baltimore County, Maryland, USA

4 Oregon State University, Oregon, USA

5 Colorado State University, Colorado, USA

Graduate Student Mathematical Modeling Camp (GSMMC)  
University of Delaware, June 2019

## Abstract

Membrane filters are used in various industrial engineering processes and one of the most significant applications is water purification, where target particles, colloids and macromolecules, are removed from the water flow by applying microfiltration. Hence mathematical models to predict their efficacy are potentially very useful, as such models can suggest design modifications to improve filter performance and lifetime. Many models have been proposed to describe particle capture by membrane filters and the associated fluid dynamics, but most of such models are based on a very simple structure in which the pores of the membrane are assumed to be simple circularly cylindrical tubes spanning the depth of the membrane. Real membranes used in applications can have much more complex internal structure, with interconnected pores that may branch and bifurcate, and pore-size variation across the membrane. However, during the filtration process, membrane fouling due to the block of large particles and deposition of small particles occur and decreases the membrane performance. Thus, the membrane's permeability decreases as the filtration progresses. Two driving mechanisms can be considered an here: (i) constant pressure drop across the membrane specified; and (ii) constant flux through the membrane specified. In the former case the flux will decrease in time as the membrane becomes fouled; in the latter, the pressure drop required to sustain the constant flux will rise as fouling occurs. Considering elasticity to sub-branches in constant flux scenario, in some stage of filtration process, the radius of pores may tend to expand due to the effect of high pressure on the elastic sub-branches, which is not negligible.

## 1 Introduction

Membrane filters are crucial in many industrial engineering processes. Most importantly, they are used for water purification, but other applications include air and other gas purification, treatment of radioactive sludge, and even beer purification [1]. They also show up in the biotech field, where they are used in artificial kidneys to remove toxic substances [2]. Filtration was also used to help brew your cup of coffee this morning.

Depending on the application, membrane filters could be made of various materials and geometries [1]. A few different structures are shown in figure 1. These arise from finding a balance between the control of the particle removal and minimization of the energy requirements. For consideration, a membrane with small pores such that all of the particles are filtered will require a large amount of energy to as there will be a high resistance for the flow. Hence, it is commonly used in the industry that absorption is to be responsible for a significant portion of filtration, that is, the deposition of small particles on the pore walls within membrane. That way, membranes with larger pores operating with lower pressures can be used.

The flow through membrane filters is often modeled by studying the flow through rigid pores, one of which is shown in figure 2, using Darcy's Law. This is assuming a low Reynolds number and gives the dependence of the flux through the pores from pressure. It is also usually assumed that the pores are axisymmetric, i.e, the symmetric about the axis. If the cases where the pores are treated as an elastic system, it can be assumed that the filter is the same material, and hence, has the same elastic properties as the membrane. This is a property to consider since some industrial membranes have layers of different material filters.

The goal of this work is to analyze the effects of pressure on the pore size of the filters and the concentration throughput using the preceding assumptions. In particular, we assume a superficial Darcy velocity of the fluid. The model is applied to two different cases: thick-walled cylinders and thin-walled cylinders, both of which are considered elastically. Therefore,

to derive the pore radius deformation, we use the Donnell shell theory [4] for thin-walled cylinders whereas we use the cylindrical coordinate methods for thick-walled deformation [6].

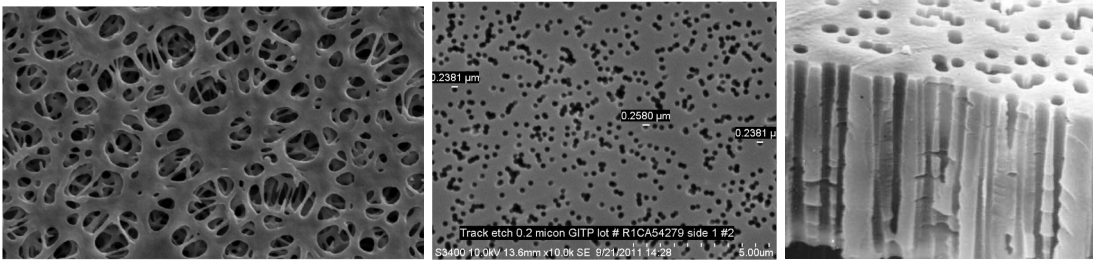


Figure 1: Membrane filters

## 2 Thick-Walled Cylinders

### 2.1

The thick-walled cylinder can be seen as shown in figure 2. Here,  $X$  is the axial direction,  $C(X, T)$  denotes the concentration of small particles,  $A(X, T)$  is the radius of the pore at  $X$  and time  $T$ ,  $D$  is the length of the pore, and  $2W$  denotes width and depth of an element of the membrane containing a single pore. We describe the deformation of the elastic membrane using Navier-Cauchy equation

$$\mu_1 \nabla^2 \mathbf{\Omega} + (\mu_2 + \mu_1) \nabla(\nabla \cdot \mathbf{\Omega}) + \mathbf{H} = \rho \frac{\partial^2 \mathbf{\Omega}}{\partial T^2}, \quad (1)$$

where  $\mathbf{\Omega} = (\Omega_R, \Omega_\theta, \Omega_X)$  is the displacement vector in cylindrical coordinates,  $\rho$  denotes the density,  $\mu_1$  and  $\mu_2$  are Lamé's first and second parameters, respectively. Lamé's parameters are given by

$$\begin{aligned} \mu_1 &= \frac{E}{2(1 + \nu)}, \\ \mu_2 &= \frac{E\nu}{(1 + \nu)(1 - 2\nu)}, \end{aligned} \quad (2)$$

where  $E$  is Young's modulus, and  $\nu$  is Poisson's ratio.

Let body force  $\mathbf{H} = \mathbf{0}$ , as we will consider the force due to pressure at the boundary conditions. Assuming an elastostatic condition (the condition of equilibrium, in which all forces on the body sum to zero), we have

$$\frac{\partial^2 \mathbf{\Omega}}{\partial T^2} = 0. \quad (3)$$

Putting equation (1), (2) and (3) together, it follows that

$$\nabla^2 \mathbf{\Omega} + 2\nu \nabla(\nabla \cdot \mathbf{\Omega}) = 0. \quad (4)$$

Write the governing equation (4) componentwisely in cylindrical coordinates,

$$\nabla^2 \Omega_R - \frac{\Omega_R}{R^2} - \frac{2}{R^2} \frac{\partial \Omega_\theta}{\partial \theta} + \frac{1}{1 - 2\nu} \frac{\partial}{\partial R} (\nabla \cdot \mathbf{\Omega}) = 0, \quad (5)$$

$$\nabla^2 \Omega_\theta - \frac{\Omega_\theta}{R^2} - \frac{2}{R^2} \frac{\partial \Omega_R}{\partial \theta} + \frac{1}{1 - 2\nu} \frac{\partial}{\partial R} (\nabla \cdot \mathbf{\Omega}) = 0, \quad (6)$$

$$\nabla^2 \Omega_X + \frac{1}{1 - 2\nu} \frac{\partial}{\partial X} (\nabla \cdot \mathbf{\Omega}) = 0, \quad (7)$$

since divergence operator and Laplacian operator in cylindrical coordinates has the form

$$\nabla \cdot \mathbf{\Omega} = \frac{1}{R} \frac{\partial}{\partial R} (R\Omega_R) + \frac{1}{R} \frac{\partial \Omega_\theta}{\partial \theta} + \frac{\partial \Omega_X}{\partial X}, \quad (8)$$

$$\nabla^2 \Omega_i = \frac{1}{R} \frac{\partial}{\partial R} \left( R \frac{\partial \Omega_i}{\partial R} \right) + \frac{1}{R^2} \frac{\partial^2 \Omega_i}{\partial \theta^2} + \frac{\partial^2 \Omega_i}{\partial X^2}. \quad (9)$$

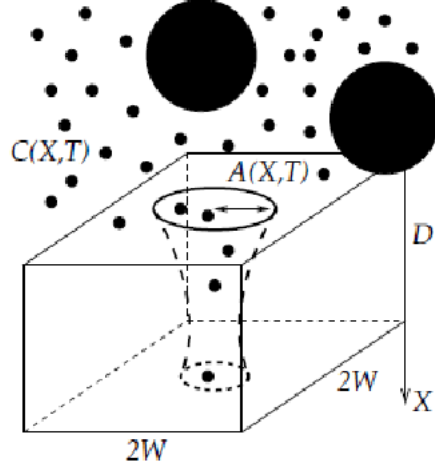


Figure 2: Schematic showing the single unit of membrane, assumed repeated in a square lattice. Small particles, at concentration  $C(X, T)$ , which enter pores and deposit within, are indicated, as are large particles, which block the pore inlet.

Note that  $\Omega_\theta = 0$  due to the axisymmetric geometry. Denote  $\mathbf{n}$  the normal vector to the pore wall, and note that it is parallel to  $\nabla(R - A) = \left( \frac{\partial(R-A)}{\partial R}, 0, \frac{\partial(R-A)}{\partial X} \right) = (1, 0, -\frac{\partial A}{\partial X})$ . Furthermore,

$$\Sigma_R = \frac{E(1-\nu)}{(1+\nu)(1-2\nu)} \frac{\partial \Omega_R}{\partial R} + \frac{E\nu}{(1+\nu)(1-2\nu)} \frac{1}{R} \left( \frac{\partial \Omega_\theta}{\partial \theta} + \Omega_R \right) + \frac{E\nu}{(1+\nu)(1-2\nu)} \frac{\partial \Omega_X}{\partial X}, \quad (10)$$

$$\Sigma_\theta = \frac{E\nu}{(1+\nu)(1-2\nu)} \frac{\partial \Omega_R}{\partial R} + \frac{E(1-\nu)}{(1+\nu)(1-2\nu)} \frac{1}{R} \left( \frac{\partial \Omega_\theta}{\partial \theta} + \Omega_R \right) + \frac{E\nu}{(1+\nu)(1-2\nu)} \frac{\partial \Omega_X}{\partial X}, \quad (11)$$

$$\Sigma_X = \frac{E\nu}{(1+\nu)(1-2\nu)} \frac{\partial \Omega_R}{\partial R} + \frac{E\nu}{(1+\nu)(1-2\nu)} \frac{1}{R} \left( \frac{\partial \Omega_\theta}{\partial \theta} + \Omega_R \right) + \frac{E(1-\nu)}{(1+\nu)(1-2\nu)} \frac{\partial \Omega_X}{\partial X}. \quad (12)$$

We would like to scale all of the variables to render the equations dimensionless. We introduce the following change of variables

$$X = Dx, \quad A = Wa = \varepsilon Da, \quad R = Wr = \varepsilon Dr, \quad (\Omega_R, \Omega_\theta, \Omega_X) = W(\omega_r, \omega_\theta, \omega_x), \quad (\Sigma, P) = \frac{8\mu D Q_{pore}}{\pi W^4}(\sigma, p), \quad (13)$$

where  $\varepsilon := \frac{W}{D} \ll 1$ .

The axisymmetric assumption gives  $\Omega_\theta = 0$  and therefore there is no  $\theta$ -dependency. We rewrite equations (5), (6), and (7) using (8), (9) and (13) and get

$$\frac{1}{\varepsilon D} \left\{ \frac{1}{r} \frac{\partial}{\partial r} \left( r \frac{\partial \omega_r}{\partial r} \right) + \frac{1}{r^2} \frac{\partial^2 \omega_r}{\partial \theta^2} + \varepsilon^2 \frac{\partial^2 \omega_r}{\partial x^2} - \frac{\omega_r}{r^2} - \frac{2}{r^2} \frac{\partial \omega_\theta}{\partial \theta} + \frac{1}{1-2\nu} \frac{\partial}{\partial r} \left[ \frac{1}{r} \frac{\partial}{\partial r} (r\omega_r) + \frac{1}{r} \frac{\partial \omega_\theta}{\partial \theta} + \varepsilon \frac{\partial \omega_x}{\partial x} \right] \right\} = 0, \quad (14)$$

$$0 = 0, \quad (15)$$

$$\frac{1}{\varepsilon D} \left\{ \frac{1}{r} \frac{\partial}{\partial r} \left( r \frac{\partial \omega_r}{\partial r} \right) + \varepsilon^2 \frac{\partial^2 \omega_x}{\partial x^2} + \varepsilon \frac{1}{1-2\nu} \frac{\partial}{\partial x} \left[ \frac{1}{r} \frac{\partial}{\partial r} (r\omega_r) + \varepsilon \frac{\partial \omega_x}{\partial x} \right] \right\} = 0. \quad (16)$$

Extracting the leading order terms of equation (14) and (16), we get

$$\frac{1}{r} \frac{\partial}{\partial r} \left( r \frac{\partial \omega_{0r}}{\partial r} \right) - \frac{\omega_{0r}}{r^2} + 2\nu \frac{1}{r} \frac{\partial}{\partial r} (r\omega_{0r}) = 0, \quad (17)$$

$$\frac{1}{r} \frac{\partial}{\partial r} \left( r \frac{\partial \omega_{0x}}{\partial r} \right) = 0. \quad (18)$$

The boundary conditions are

$$\Sigma_R \Big|_{R=A} = P, \quad \frac{\partial \Sigma_R}{\partial R} \Big|_{R=W} = 0, \quad (19)$$

which become

$$\sigma_r \Big|_{r=a} = p, \quad \frac{\partial \sigma_r}{\partial r} \Big|_{r=1} = 0. \quad (20)$$

The clamped boundary conditions take on the form

$$\omega_x \Big|_{x=0} = 0, \quad \omega_x \Big|_{x=1} = 0, \quad (21)$$

$$\frac{8\mu D Q_{\text{pore}}}{\pi W^4} \sigma_r = \frac{E}{(1+\nu)(1-2\nu)} \left[ (1-\nu) \frac{\partial \omega_r}{\partial r} + \nu \frac{\omega_r}{r} + \nu \epsilon \frac{\partial \omega_x}{\partial x} \right], \quad (22)$$

leading to

$$\sigma_r = \frac{\pi E W^4}{8\mu D Q_{\text{pore}} (1+\nu)(1-2\nu)} \left[ (1-\nu) \frac{\partial \omega_r}{\partial r} + \nu \frac{\omega_r}{r} + \nu \epsilon \frac{\partial \omega_x}{\partial x} \right]. \quad (23)$$

By letting  $\eta = \pi E W^4 / [8\mu D Q_{\text{pore}} (1+\nu)(1-2\nu)]$ , the first-order terms give

$$\sigma_{r_0} = \eta \left[ (1-\nu) \frac{\partial \omega_{0r}}{\partial r} + \nu \frac{\omega_{0r}}{r} \right]. \quad (24)$$

Defining  $y := \omega_{0r}$  and  $y' := \frac{\partial \omega_{0r}}{\partial r}$  allows us to obtain the ordinary differential equation

$$\frac{1}{r} (ry')' - \frac{y}{r^2} + \frac{1}{1-2\nu} \left( \frac{1}{r} (ry)' \right)' = 0, \quad (25)$$

which has the solution

$$\omega_{0r} = c_1(x)r + \frac{c_2(x)}{r}. \quad (26)$$

Hence,

$$\sigma_{r_0} = \eta \left[ (1-\nu) \left( c_1 - \frac{c_2}{r^2} \right) + \nu \left( c_1 + \frac{c_2}{r^2} \right) \right]. \quad (27)$$

Since  $\sigma_{r_0}|_{r=a} = p_0$  and  $\frac{\partial \sigma_{r_0}}{\partial r}|_{r=1} = 0$  we have

$$p_0 = \eta \left[ (1-\nu) \left( c_1 - \frac{c_2}{a^2} \right) + \nu \left( c_1 + \frac{c_2}{a^2} \right) \right], \quad (28)$$

from which

$$0 = \eta [(1-\nu)2c_2 - \nu(2c_2)]. \quad (29)$$

This allows us to conclude that

$$c_2 = 0, \quad c_1 = \frac{p_0}{\eta}, \quad \omega_{0r} = \frac{p_0 r}{\eta}. \quad (30)$$

### 3 Thin-Walled Cylinders

To analyze the flow through the membrane pore, we consider cylindrical geometry having a much smaller cross-sectional area than the “stream-wise” dimension and a negligible thickness compared to the cross-sectional dimension. In other words, apart from the assumption of steady and axisymmetric flow, we assume that the length,  $D$ , and the pore radius,  $A$ , satisfy  $A/D \ll 1$ . This is shown in figure 3.

When analyzing the membrane pore, we make use of Donnell’s Shell Theory which takes into account the bending of the membrane pore as well [4]. Though we skip the intricate details associated with the equation expressing the momentum balance, the reader is encouraged to consult DYM [5]. Also, the thickness of the pore,  $\Upsilon$ , is assumed to be small compared to the pore radius, i.e.,  $\Upsilon/A \ll 1$ .

#### 3.1 Donnell Shell Equation

Following Anand and Christov [4], we introduce elasticity in our system with the following equation

$$\frac{E\Upsilon^3}{12(1-\nu^2)} \left( \frac{\partial^4 \Omega_r}{\partial X^4} + \frac{12\Omega_r}{\Upsilon^2 A^2} \right) = P(X), \quad (31)$$

in which we substitute the dimensionless variables

$$X = Dx, \quad A = Wa, \quad \Omega_r = \frac{8\mu D Q_{\text{pore}}}{4\pi E W^3} \omega_r, \quad P = \frac{8\mu D Q_{\text{pore}}}{\pi W^4} p \quad (32)$$

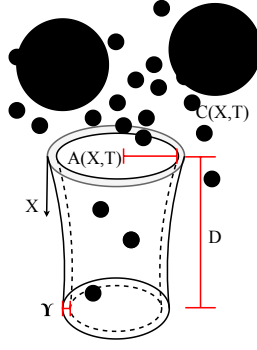


Figure 3: Schematic showing the single unit of membrane with a thin shell. Small particles, at concentration  $C(X, T)$ , which enter pores and deposit within, are indicated, as are large particles, which block the pore inlet.

in order to obtain

$$\left(\frac{\Upsilon}{a}\right)^2 \left(\frac{a}{D}\right)^4 \frac{\partial^4 \omega_r}{\partial x^4} + \frac{12\omega_r}{W^2} = \frac{12(1-\nu^2)a^2}{\Upsilon W} p. \quad (33)$$

For our thin-walled and slender shell, the relationships  $\Upsilon \ll A$  and  $A \ll D$  indicate that the partial derivative term can be neglected to the leading order in  $\Upsilon/A$  and  $A/D$ . It follows that the pore radius deformation from the terms left over is given by

$$\omega_r = \frac{(1-\nu^2)W}{\Upsilon} pa^2. \quad (34)$$

This relationship will dictate how the pore expands as its radius and the fluid pressure change.

## 4 Computations

Our goal is to use the current pore radius and pressure values to update the radius. We begin by computing the particle concentration by resolving the ordinary differential equation

$$\frac{\partial c}{\partial x} = -\tilde{\lambda}ca, \quad c(x=0, t) = 1 \quad (35)$$

and the concentration is employed in finding the radius by solving

$$\frac{\partial a}{\partial c} = -\tilde{\beta}c, \quad a(x, t=0) = a_0(x). \quad (36)$$

We use the obtained quantities to determine the number of unblocked pores using

$$\frac{dn}{dt} = \left[ -n \left( n + \frac{1-n}{1+\rho_b a^4} \right)^{-1} (1-g(a)) \right]_{x=0} \quad (37)$$

and, in turn, we solve the following integral for the pressure

$$p = \int_x^1 \frac{dx'}{a^4 [n + (1-n)/(1+\rho_b a^4)]}. \quad (38)$$

Now we seek the radial deflection value,  $\omega_r$ , which we then use in obtaining the new pore radius. There are two cases:

1. If the thick-wall model is assumed, we use the right-most of equations equation (30). The updated radius is obtained with the previous radius and pressure values:

$$a \leftarrow a + \omega_{0r} \Big|_{r=a} = a + \frac{pa}{\nu}. \quad (39)$$

2. If the thin-wall model is assumed, we use instead equation (34). The updated radius is obtained with the previous radius and pressure values:

$$a \leftarrow a + \omega_r \Big|_{r=a} = a + \frac{Wpa^2}{\Upsilon}. \quad (40)$$

Equipped with the next-step radius, we repeat the entire process above to uncover the subsequent radii.

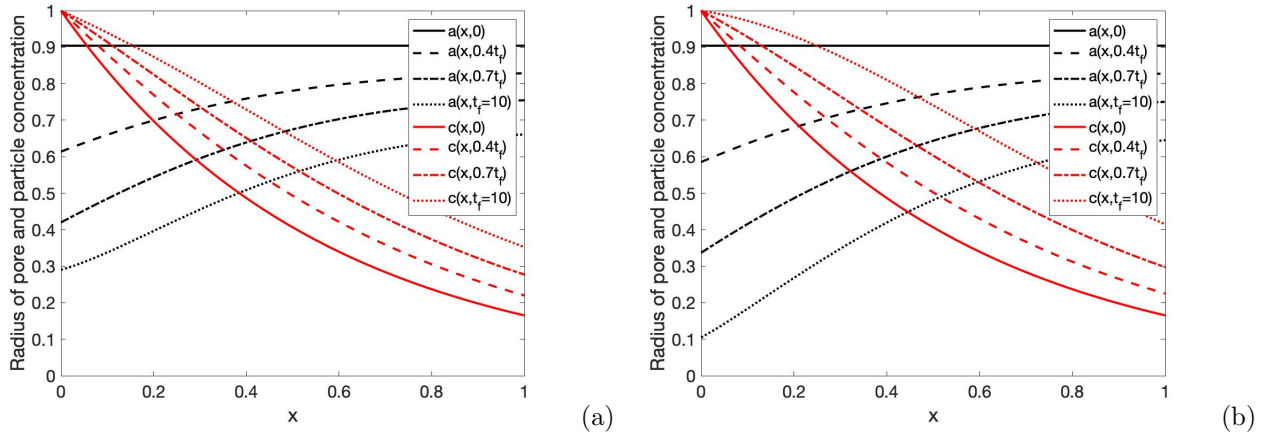


Figure 4: (a) is the pore radius and particle concentration at selected times up to 10 under thick wall model, as indicated in the legends; (b) is the pore radius and particle concentration at selected times up to 10 under thin wall model, as indicated in the legends. Both simulations are for uniform initial pore radius profiles  $a(x, 0) = 0.904$ .

## 5 Results

We will present and illustrate some results that we get from simulation of both thick wall and thin wall model as we introduced in section §2 and 3. In section 5, we will first demonstrate how small particle concentration and pore radius evolve during the filtration process considering membrane elasticity in a constant flux scenario; then, we will show filtration performance changes when we switch between constant flux and a constant pressure scenario. Our model has several dimensionless parameters:  $\lambda$ , which captures the physics of the attraction between particles and the pore wall and  $\beta$ , which describes the pore radius shrinkage. While conducting the simulations, we used the same assumptions on values of dimensionless parameters proposed by Sanaei and Cummings [1]. Therefore we fixed the additional resistance  $\rho_b = 2$  and distribution of large-particle sizes  $g(a)|_{x=0} = 0$  in equation (37). In reality, the values of these parameters vary in different applications and different membrane materials; however, we believe that our models can give reliable predictions when detailed data from industries are given. We considered a uniform initial pore profile where pore radius is characterized by  $a(x, 0) = 0.904$ . Although we run simulations for uniform pore profile, our model can be easily applied to any axisymmetrical pore profile.

We used numerical methods to solve the model and stopped the model when the pore shrinks to zero ( $a \rightarrow 0$ ), since the membrane is not permeable anymore and the flux through it drops to zero at the stopping time  $t = t_f$ . The numerical scheme employed is center in space, backward in time, based on second-order accurate finite difference spatial discretization of the equations, with a simple implicit time step. For equations that involved integrals, trapezoidal quadrature were employed.

Figure 4 shows the pore radius  $a(x, t)$  and the concentration of small particles  $c(x, t)$  up to 10 in both models. From both figures, pore radius shrinks more in pore inlet, which is consistent with the shrinkage feature in Sanaei and Cummings results [1]. It needs to be noticed that the filtration process does not stop at time 10, since the radius is not 0, but if we let the process to continue, the displacement of the membrane would be too large and the pressure needed to sustain the flow would be too large.

As Figure 5 shows, the pressure needed at the pore inlet of both models are increasing quickly. Since the pressure is dimensionless and should be at order 1, we considered the pressure at 10 to be the maximum pressure that we apply to the filtration. Hence, as long as the pressure exceeds 10, we maintained the pressure at pore inlet to be 10 for all the following filtration processes until the final stopping time. If we maintained the pressure in the upstream, the scenario would be switched to a constant pressure instead of constant flux mentioned in the previous sessions. Sanaei and Cummings [1] studied the constant pressure scenario and proposed mathematical models in this condition. Hence, we switched between two kinds of models in the simulation and presented the results in Figure 6.

In Figure 6(a), the thick wall model is firstly considered to simulate the constant flux scenario. The curves with respect to early filtration process, for example, at time 0 and  $0.4t_f$ , the evolution of particle concentration, and radius shrinkage are consistent with Figure 4. After the switching of the model, the radius at the final filtration stage expands a little bit, which is indicated at the cross of the two curves. The same situation also appears at the simulation of the thin wall model. However, the expansion of the radius at the final stage in the thick wall model is more than the thin wall model. The final stopping time for the thick wall model is 11.025 and the stopping time for the thin wall model is 9.975.

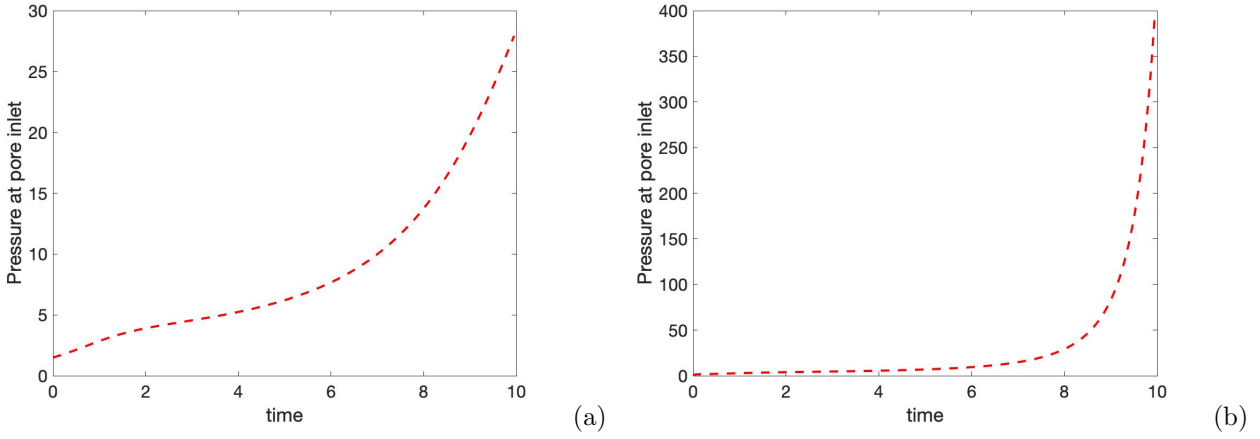


Figure 5: (a) is the evaluation of pressure in thick wall model in 10; (b) is the evaluation of pressure in thin wall model in 10.

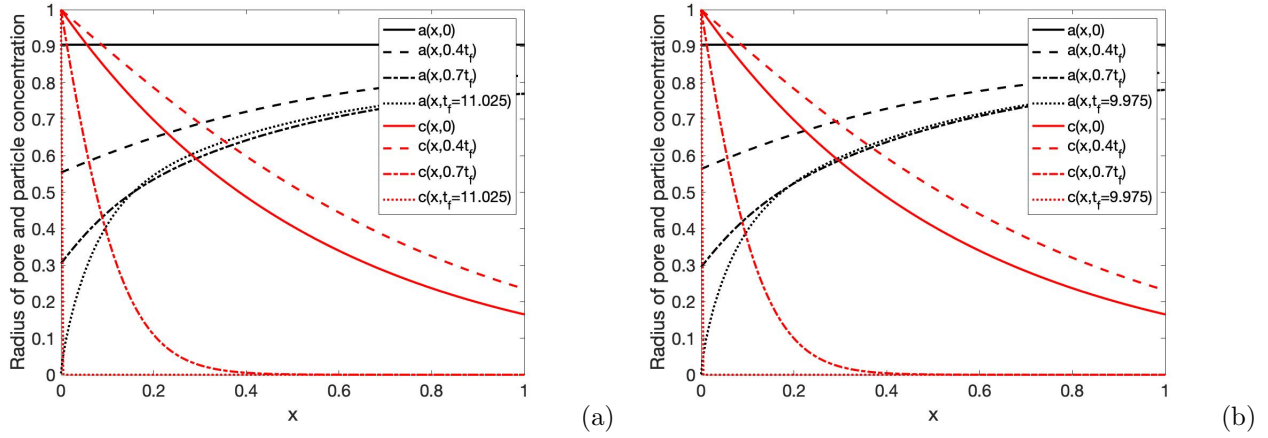


Figure 6: (a) is the pore radius and particle concentration at selected times up to the final blocking time ( $t_f = 11.025$ ) under thick wall model, as indicated in the legends; (b) is the pore radius and particle concentration at selected times up to the final blocking time ( $t_f = 9.975$ ) under thin wall model, as indicated in the legends. Both simulations are for uniform initial pore radius profiles  $a(x, 0) = 0.904$

## 6 Future Work

Our model represents an interesting result for internal membrane complexity, but the real membranes are much more complicated in their structure than our simple assumptions. They may consist of many randomly oriented pores, which branch and reconnect [2] (Figure 7), so that the solution becomes difficult through the membrane rather than the simple flow assumed here. In the future, we can consider more sophisticated models, which include branching and reconnecting pores, to better account for such internal membrane complexity with multiple membrane fouling modes (including so-called cake filtration, which occurs normally at a late stage of the filtration process). We considered cylindrical pores here and due to elasticity, the geometry of the pores may change after a certain amount of time. Therefore, we can make some predictions on what type of membrane might offer optimal filtration performance.

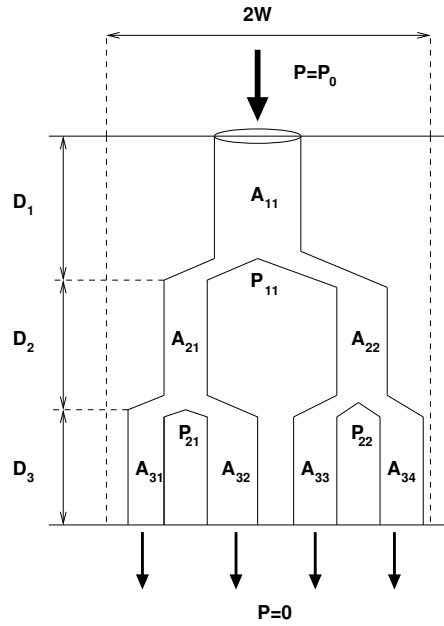


Figure 7: Filters with branches

## References

- [1] P. Sanaei and L. J. Cummings, *Flow and fouling in membrane filters: effects of membrane morphology*, *Journal Fluid Mechanics* **818** (2017), 744-771.
- [2] Pejman Sanaei and Linda J. Cummings, *Membrane filtration with complex branching pore morphology*, *Physics Review Fluids* **3** (2018).
- [3] Ivan C. Christov, Vincent Cognet, Tanmay C. Shidhore, and Howard A. Stone, *Flow rate-pressure drop relation for deformable shallow microfluidic channels*, *Journal of Fluid Mechanics* **841** (2018), 267-286.
- [4] Vishal Anand and Ivan C. Christov, *Steady low Reynolds number flow of a generalized Newtonian fluid through a slender elastic tube*, *Arxiv* (2018), available at <https://arxiv.org/abs/1810.05155>.
- [5] C. L. Dym, *Introduction to the Theory of Shells*, New York, NY: Hemisphere Publishing Corporation, 1990.
- [6] Stephen P. Timoshenko and Sergius Woinowsky-Krieger, *Theory of plates and shells*, McGraw-Hill, 1959.